ELSEVIER

International Journal of Mass Spectrometry 178 (1998) 161–171

International Journal of Mass Spectrometry

High-pressure flowing-afterglow setup validated by the study of the CO_3^- + HNO_3 reaction

C. Guimbaud[1], D. Labonnette, V. Catoire*, R. Thomas

Laboratoire de Physique et Chimie de l'Environnement, UPR n°4010 du CNRS conventionnée avec l'Université d'Orléans, 3A Av. de la Recherche Scientifique, 45071 Orléans Cedex 2, France

Received 30 April 1998; accepted 23 July 1998

Abstract

A high-pressure flowing-afterglow apparatus has been built in order to study in the laboratory gas-phase reactions of ions with neutral molecules playing an important role in the stratospheric ozone chemistry. The instrument consists of a flow tube, a first intermediate pressure chamber located between two conical electrodes, a quadrupole guide in a second intermediate pressure chamber, and a quadrupole mass analyzer in a third chamber. A method of measurement of the residence time for the ions in the flow tube has been used to derive absolute reaction rate coefficients. The validation of this setup was performed at room temperature over a pressure range of 1–3 hPa by the study of the well-known reaction CO_3^- + HNO_3. The rate coefficient was measured as $(1.2 \pm 0.3) \times 10^{-9}$ cm^3 s^{-1}, and $CO_3^-(HNO_3)$, NO_3^-, and $NO_3^-(OH)$ were detected as primary product ions, in agreement with results previously reported. For the first time, the study was extended up to 24 hPa and at lower temperature. The rate coefficient was found to be independent of pressure above 1.1 hPa, but increased to a value of $(2.4 \pm 0.7) \times 10^{-9}$ cm^3 s^{-1} at 212 K. The relative yield of $CO_3^-(HNO_3)$ increased with pressure to a value $\geq$ 60% above 12 hPa at 298 K, and $\geq$ 85% above 6 hPa at 212 K. These results are fundamental to the derivation of a HNO_3 mixing ratio in the stratosphere with balloon-borne instruments using active chemical ionization mass spectrometry. (Int J Mass Spectrom 178 (1998) 161–171) © 1998 Elsevier Science B.V.

Keywords: Flowing afterglow; Ion/molecule reaction; HNO_3; Stratosphere

1. Introduction

Aircraft and balloon-borne mass spectrometry measurements of natural gaseous ions in the atmosphere were used in the past to detect neutral trace species. The ion/neutral molecule reactions involved give indeed specific ionic products [1,2]. This passive detection method has now been superseded by active chemical ionization mass spectrometry, in which ions are generated in the stratosphere, by using embarked ion sources [3,4]. Presently a balloon-borne instrument called MACSIMS (measurement of atmospheric constituents by selective ion mass spectrometry) is developed using this technique, with the aim of detecting stratospheric trace constituents such as HNO_3 and $ClONO_2$ in relation with ozone chemistry [5]. This instrument was realized within the framework of a European program, and is a collaboration between the Belgisch Instituut voor Ruimte Aërono-

* Corresponding author. E-mail: Valery.Catoire@univ-orleans.fr

[1] Present address: Department of Earth, Atmospheric and Planetary Sciences, Massachusetts Institute of Technology, Cambridge, MA 02139.

PII S1387-3806(98)14115-5

mie (BIRA) in Brussels, the Physikalisches Institut Universität Bern (PIUB), and our laboratory in Orléans (LPCE). It consists of a flow tube, including ion sources, associated with a double focusing mass spectrometer of Mattauch-Herzog geometry, and an octopole guide in an intermediate pressure chamber [6] to allow measurements at stratospheric pressures. In parallel, a flowing-afterglow apparatus was built at the BIRA [7,8] to study ion/molecule reactions involved in the analysis of the in-situ data of MACSIMS. The BIRA instrument, however, does not allow measurements above few hPa.

Results of MACSIMS balloon flights have shown the influence of stratospheric pressure on the nature of the primary clustering ions generated by the ion sources and on the kinetics of the involved ion/molecule reactions [4]. Therefore, it appeared necessary to us to build a high-pressure (1–100 hPa) laboratory apparatus in order to refine the interpretation of the flight data and to define the best ion sources and primary ions to be used in the future flights. This new instrument, comprising two intermediate pressure chambers between the flow tube and the mass analyzer, is described in the present paper. Its principle is based on the flowing-afterglow technique, originally developed in the NOAA laboratory [9].

Rate coefficients of ion/molecule reactions may be determined by relative measurements using different reference reactions which are not always well characterized. In this case, discrepancies are frequently observed between the rate coefficient values reported by authors for a given ion/molecule reaction [10]. Our apparatus enables the derivation of absolute rate coefficients, as the concentration of the reactive neutral species and the residence time of the ions in the flow tube are both measured. The ion residence time cannot simply be derived from the average value of the carrier gas velocity, as was illustrated by Upschulte et al. [11], who obtained a wide range of values (0.8–1.6) for the ratio of the average ion velocity to the average carrier gas velocity, noted V_i/V_g, under various conditions (i.e. the dynamic of the carrier gas flow, the flow tube radius). Previous experimental and theoretical investigations of the dynamic of the carrier gas and ion flow also showed that this ratio requires an experimental determination [9,12].

The study of the reaction CO_3^- + HNO_3 was chosen to validate our new flowing-afterglow setup. Two relative determinations of the rate coefficient have already been performed at room temperature and low pressure ($\leq$ 3 hPa), by Fehsenfeld et al. [13], and Möhler and Arnold [14]. Using the recent values of Huey [15] for the reference reactions, a good agreement is obtained between their measured values: (1.4 $\pm$ 0.4), and (1.6 $\pm$ 0.6), in units of 10^{-9} cm^3 s^{-1}, respectively. In addition, Möhler and Arnold [14] studied the product ion distribution between 1 and 3 hPa, and mentioned an increase of the yield for the primary product ion $CO_3^-(HNO_3)$ with increasing pressure, relative to the NO_3^- and $NO_3^-(OH)$ yields. To confirm these results and to test the ability of our apparatus to work over a wide range of pressure, absolute kinetic and product study of the above reaction was carried out between 1.1 and 24.3 hPa. Furthermore, rate coefficient and product yields were determined at temperatures similar to those of the stratosphere.

2. Experimental

The new apparatus is shown in Fig. 1. It consists of a flow tube, including ion sources, where ion/molecule reactions take place, and three differentially pumped chambers, where the ions are sampled and mass analyzed.

2.1. Flow tube and UV-absorption system

The flow tube is a stainless steel cylinder of 100 cm long and 3.5 cm i.d. (inner diameter). The use of metal as a construction material allows the neutralization of the ions at the walls. A flow of carrier gas (N_2, purity $\geq$ 99.999%) is established by a 500 m^3 h^{-1} roots blower pump backed by a 65 m^3 h^{-1} rotary vane pump. The carrier gas is regulated from 1 to 100 slm (standard liter per minute) by a mass flowmeter (MKS), resulting in pressures of 0.5–50 hPa in the flow tube. The fast flow of around 50 m s^{-1} is

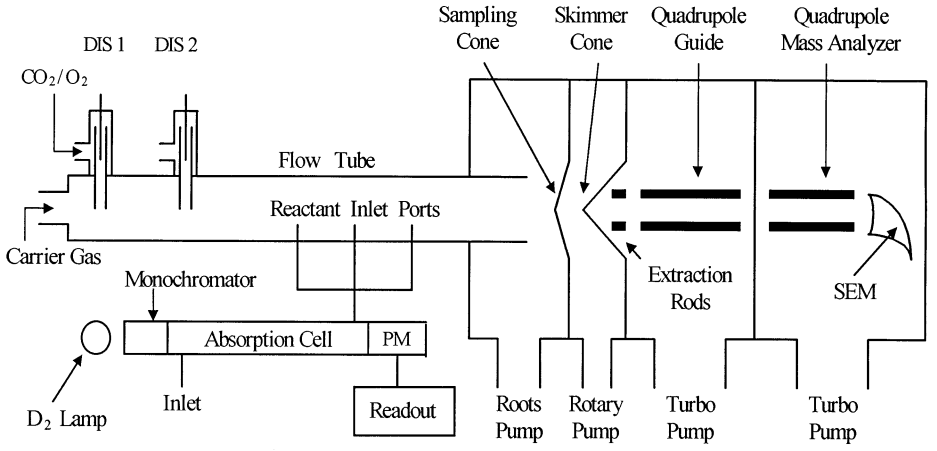

Fig. 1. Overview of the high-pressure flowing-afterglow setup.

maintained up to 30 hPa by the pumping, and is reduced above this pressure. Primary negative ions such as CO_3^- are generated in a discharge ion source (DIS). They are produced by a dc discharge maintained by a high voltage (1500 V) applied between a molybdenum needle and a cylindrical stainless steel capillary tube (0.4 cm i.d.). Two ion sources of similar design are installed. The outlets of their capillary, through which the ions are injected into the flow tube axis, are located at distances of 108.6 and 87.5 cm upstream of the sampling cone.

The neutral species of interest in stratospheric chemistry which are planned to be studied (e.g. HNO_3, $ClONO_2$, N_2O_5, O_3) all absorb ultraviolet radiation. A UV-absorption system was thus mounted upstream of the flow tube. It includes a 51 cm long × 2 cm i.d. glass absorption cell, fitted with suprasil windows, and connected to the flow tube by a stainless steel tube with three inlet ports of 0.4 cm i.d. The intensity of a UV beam, coming from a deuterium lamp (Oriel) and filtered by a grating monochromator, is measured at the exit of the absorption cell by a photomultiplier (Oriel) connected to an amplifier-readout system. The gaseous phase of the reactant neutral species is carried by a known flow of the carrier gas through the absorption cell using a flowmeter (MKS). Its concentration in the cell is derived by Beer-Lambert's law, knowing the absorption cross-section $\sigma(\lambda)$ at the analysis wavelength λ. The technical characteristics of the deuterium lamp and the photomultiplier allow measurements between 190 and 350 nm. The neutral species enters the flow tube through one of the three inlets, located 20, 40, and 60 cm downstream of the nearest DIS (DIS2 in Fig. 1), corresponding to reaction distances of 67.5, 47.5 and 27.5 cm. The minimal distance between this DIS and the first inlet is sufficient to ensure that all electrons or excited primary ions generated are lost or stabilized by collisions, respectively [8]. At the downstream end of the flow tube, ions are collected by an electrically insulated positively biased (1–3 V) sampling cone.

2.2. Sampling, focusing, and mass analyzing zones

As mass analyzer, a quadrupole mass spectrometer was used (Balzers QMG 421 C-4), which required working pressures of less than 10^{-5} hPa. At least one intermediate pumping chamber is necessary to lower the pressure gradually from around 100 hPa in the flow tube to below 10^{-5} hPa in the quadrupole mass spectrometer. A multipole guide (operating in rf mode only) is suitable for this purpose because (i) it transfers ions over a long distance (a few 10 cm), offering space for a great pumping efficiency, and (ii) it needs lower energy (< 50 eV) for the ions than electrostatic lenses, allowing the quadrupole analyzer to operate properly. A quadrupole, pumped with a 200 L s^{-1} turbomolecular pump, was chosen as multipole

guide. Its mechanical characteristics are less critical than an octopole, which renders its building easier. To minimize ion loss, the mean free path of the ions has to be at least equal to the length of the quadrupole guide rods. This results in a maximum pressure of 10^{-4} hPa for a transfer length of about 20 cm in this quadrupole guide. Under this pressure conditions, a 10 μm inlet aperture would have been required to decrease the pressure from around 100 to 10^{-4} hPa. Such an orifice is easily polluted and blocked up. Therefore, another intermediate pumping chamber was added between the flow tube and the quadrupole guide. This chamber is pumped by two rotary vane pumps (40 $m^3\ h^{-1}$), giving pressures of about 10^{-1}–1 hPa for pressures of typically 10–100 hPa in the flow tube. It allows the guiding of the ions over a 0.4 cm length path, through a dc electrostatic field located between two positively biased cones, called sampling and skimmer cones.

A series of experiments was performed to optimize the ion transfer from the flow tube to the entrance of the mass analyzer. The best result obtained was a maximum current of 10^5 ions s^{-1} collected in this latter zone by a 3000-V biased channeltron backed by a ratemeter, for a pressure of 10 hPa in the flow tube. The conditions were the following. A conical tube of 1.9 cm i.d. was mounted on the end of the flow tube; a sampling cone ended by a thin (0.2 mm) plate and a skimmer cone, with orifices of 0.2 and 1.5 mm i.d., respectively, were used to minimize ion losses on the orifice sides. This geometric set, combined to a few volts applied on the sampling cone (1–3 V) and between the two cones (5–10 V), was found to be the most efficient for collecting ions. This shows that electrostatic effects are of limited importance with respect to collisional effects, which confirms that the ion flow is still viscous in the first chamber. In contrast, the pressure in the quadrupole guide is low enough, so that the flow becomes molecular and ion transfer was efficiently achieved by electrostatic means. Each of the four 23-cm long quadrupole rods was extended towards the skimmer cone by an insulated 4.7 cm long rod with a conical tip to deeply enter this cone. A dc voltage was applied on these four short rods and gives to them an extraction lens behavior. The field axis between these extraction rods (15–50 V) is independent from that of the quadrupole rods itself (10–25 V). The usefulness of the short rods was predicted by simulation with SIMION ion package [16], and confirmed by the increase to a maximum of 10^5 ion s^{-1} for the ion current measured at the exit of the quadrupole guide. This exit consists of a 0.3 cm i.d. orifice of a positively-biased ($\approx$30 V) inlet plate, through which ions enter the mass analyzer chamber. This one is pumped with a 140 L s^{-1} turbomolecular pump. Ions are separated by the quadrupole mass spectrometer (50–60 V of field axis) and detected with a secondary electron multiplier (SEM). For a flow tube pressure of 10 hPa, the pressure in this chamber is around 10^{-6} hPa. A maximum of 10^3 ions s^{-1} was detected at the exit of the mass spectrometer, which operates in the ion counting mode.

At the present time, the DIS yield and the ion transmission efficiency are high enough to study ion/molecule reactions up to around 20 hPa. The validation of the instrument under the configuration above was carried out, which implies measurements of rate coefficients giving results in agreement with previous studies.

2.3. Reaction time measurement

To measure absolute values of rate coefficients, the reaction time τ between the molecules and the ions has to be known. It is deduced from the equation $\tau = d/v_{ion}$, where d is the reaction distance and v_{ion} the velocity of the ions sampled, the latter being derived from measurements of the ion residence time. The method of measurement consists in pulsing the DIS and synchronously recording the resulting negative ion current on the positively biased sampling cone (Fig. 2). The DIS is switched on by a pulse generator (Tektronix PG 508) via a fast high voltage transistor switch (Behlke HTS 31) of 5-μs rise time. The current is measured by a floating electrometer (Keithley 428) using a current amplification V/A of 10^{10} and a rise time of 0.3 to 1.0 ms, and visualized on a digitizing oscilloscope (Hewlett Packard 54501A). The short rise time required for not disturbing the measurement, and the low values of the current intensity ($\leq 10^{-11}$

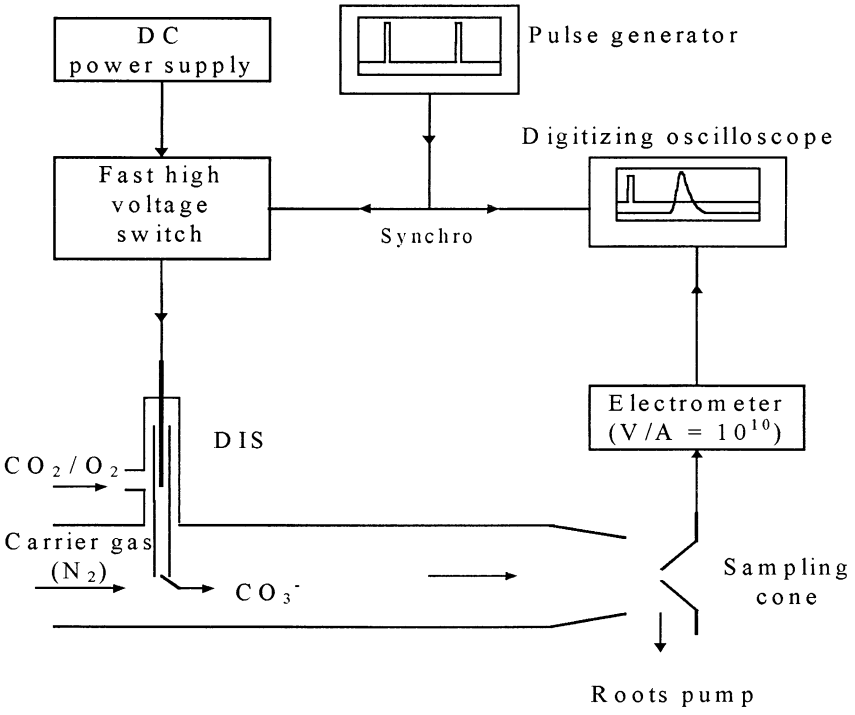

Fig. 2. Schematic of the laboratory setup used for ion residence time measurement.

A) imply that special care was taken to reduce electromagnetic noise and grounding problems. The signal recorded on the whole area of the sampling cone had an almost symmetrical, broadened shape [full width at half maximum (FWHM ≈ 4 ms)] compared to the initial pulse (1 ms), which may be principally due to longitudinal diffusion of the ions in the flow tube [12]. We considered the time corresponding to the maximum signal as the average residence time of the ions in the flow tube, and used it to infer the reaction time.

The validity of this residence time measurement method was backed up by the followings points: (i) No significantly different behavior was observed when residence time measurements were recorded with the switching-off of the DIS. So, the delay for ion generation is negligible with respect to the residence time; (ii) The average ion velocities were found to be equal to within ± 10% using residence times measured from DIS1 or DIS2 to the sampling cone or between DIS1 and DIS2. Thus, the residence time of the ions in the DIS is also negligible, and the velocity of the ions is constant in the flow, which justifies the assumption of proportionality between reaction time and reaction distance; (iii) The ratio V_i/V_g (average ion velocity/average carrier gas velocity), decreased from 1.45 to 1.12 when pressure increased from 1.1 to 24.3 hPa, as shown in Table 1. This behavior is in agreement with the results reported by Adams et al.

Table 1
Residence time of the ions (t) and ratio of the average ion velocity to the average carrier gas velocity (V_i/V_g) as a function of pressure (P_{FT}) in the flow tube

P_{FT} (hPa)	F^0_{FT} (sLm)[a]	t (ms)	V_i (m s^{-1})[b]	V_i/V_g
1.1	2.6	17	64	1.45
1.9	4.6	16.5	66	1.39
3.3	8.6	16.5	66	1.33
4.8	12.6	17	64	1.27
6.9	18.6	17	64	1.24
11.9	30.6	18	60	1.22
17.7	45.6	19	57	1.16
24.3	60.6	20	54	1.12

[a] Total flow of gases (in standard liter per minute).
[b] CO_3^- ions were used, carried by N_2 over a total distance of 108.6 cm.

and Smith and Adams [12,17]. At the lowest pressures, the flow regime is laminar and the radial velocity profile of the carrier gas is parabolic. A great part of the ions is lost at the walls, implying that most of the ions collected on the sampling cone are located near to the axis of the flow tube. Their instantaneous velocity is close to the maximum of the carrier gas velocity, i.e. twice the average carrier gas velocity V_g, but their average velocity V_i is lower because a rapid radial mixing occurs as they move along the flow tube [12]. So, the average ion velocity V_i is radially independent and can be derived from the average residence time measured. With increasing pressures, the flow regime is intermediate between laminar and turbulent, the latter occurring theoretically above 18 hPa in our flow tube (corresponding to a Reynolds number above 2000), and the ratio V_i/V_g decreased to 1.12 at 24.3 hPa. These lower values of the ratio may suggest that the radial averaging process of the ions occurs over a smaller diameter due to lesser diffusion under high-pressure laminar flow conditions, or that eddies mix all the species under turbulent flow conditions [18].

2.4. Experimental conditions for the study of the CO_3^- + HNO_3 reaction

CO_3^- primary ions were produced using a mixture of CO_2 ($\geq$ 99.9995%) and O_2 ($\geq$ 99.998%) as parent gases. Typical values for the gas flows through the ion source were 3 sccm (standard cubic centimeter per minute) of CO_2 and 600 sccm of O_2. The DIS typically generated CO_3^- ions (95%) and traces of CO_4^- (5%) ions. HNO_3 samples were prepared from commercial HNO_3 (purity $\geq$ 99.6%) mixed in H_2SO_4 (volume ratio of 1:2), vacuum distilled to remove water traces, and stored in the dark in a glass trap at −60°C. Before each use, the HNO_3-containing trap was pumped for a short time to eliminate volatile impurities, mainly NO_2. Mass spectra were a useful mean to ensure that these impurities were removed, by observing the decrease of the NO_3^- primary product peak of the reaction between NO_2 and CO_3^- [19]. In addition, the purity of HNO_3 was checked by measuring its vapor pressure versus temperature. The gaseous phase of HNO_3 was carried to the absorption cell and flow tube by bubbling a constant argon flow through the trap containing the liquid phase in a temperature-controlled bath varying from −20 to +15°C. HNO_3 concentration in the flow tube, in cm^{-3}, was given by the equation

$$[HNO_3] = [HNO_3]_{AC} \frac{F_{AC}\, P_{FT}}{P_{AC}\, F_{FT}}$$

where $[HNO_3]_{AC}$ is the concentration in the absorption cell (cm^{-3}), P_{AC} and P_{FT} are the pressures in the absorption cell and flow tube, and F_{AC} and F_{FT} are the total flows through the absorption cell and flow tube, respectively.

HNO_3 was introduced in excess (5×10^9 to 3×10^{11} cm^{-3}) in the flow tube compared to the primary ions, estimated to be 10^6–10^7 cm^{-3} by measuring the ion current on the sampling cone. The rate coefficient k (cm^3 s^{-1}) of the ion/molecule reaction was thus determined by the pseudo-first-order kinetic relationship

$$\ln([CO_3^-]/[CO_3^-]_0) = -k \times [HNO_3] \times \tau$$

where τ is the reaction time (s), and $[CO_3^-]$ and $[CO_3^-]_0$ are the ion count rates (s^{-1}), proportional to the ion concentrations, collected on the mass analyzer in the presence and absence of HNO_3, respectively. The ratio $[CO_3^-]/[CO_3^-]_0$ was varied between 90% and 10% by increasing the HNO_3 concentration. In this way, the effect of HNO_3 desorption from the walls was minimized. $[CO_3^-]$ at a given HNO_3 concentration, and $[CO_3^-]_0$ were determined alternatively, resulting from the accumulation of 200 spectra over 1 min. This was found to be the best compromise between limiting production and transmission variations of the ion quantity and improving the signal-to-noise ratio.

3. Results and discussion

3.1. Rate coefficient

The rate coefficient of the reaction CO_3^- + HNO_3 was determined at room temperature over a range of

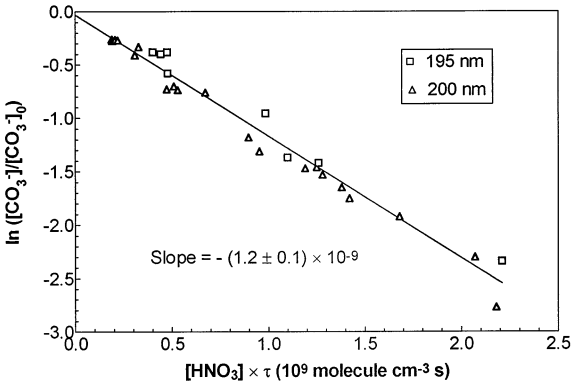

Fig. 3. Relative decay of CO_3^- signal vs. $[HNO_3] \times \tau$ at 1.9 hPa for two analysis wavelengths.

pressures of 1.1–17.7 hPa. In a first stage, reproducibility of the results obtained was tested. Two analysis wavelengths were used to check the validity of HNO_3 concentration measurement. In Fig. 3 the decay of the CO_3^- signal versus $[HNO_3] \times \tau$ is shown at 1.9 hPa, using absorption cross section $\sigma(HNO_3)$ varying by almost a factor of two, from 5.88×10^{-18} cm^2 at 200 nm to 1.02×10^{-17} cm^2 at 195 nm [20]. No effect on the rate coefficient (equal to the opposite of the slope of the plot) was discernible, giving a global value of $(1.2 \pm 0.1) \times 10^{-9}$ cm^3 s^{-1}, where the uncertainty is only statistical (confidence level of 95%). No dependence of the rate coefficient on the reaction distances used (67.5, 47.5, and 27.5 cm) was observed either. This indicates that we can neglect the inlet effects caused by the addition of neutral species which need time to diffuse into the flow stream and achieve uniform distribution [9]. Finally, electrostatic conditions of ion focusing in the transfer zone were varied, and showed no systematic dependence of the rate coefficient, giving, for example, $(1.2 \pm 0.4) \times 10^{-9}$ cm^3 s^{-1} at 4.8 hPa ($\lambda = 195$ nm, reaction distance of 67.5 cm). Only the experimental scatter increased to a value which was the highest of all experiments. In all cases, intercepts were zero, within statistical uncertainties (confidence level of 95%). Perturbation due to the perpendicular introduction of a HNO_3 flow (< 50 sccm) has therefore a negligible consequence on the CO_3^- signal, which otherwise would have been reduced and given a negative intercept. This kind of observation has been made when neutral flows above 100 sccm carrying no reactive species are introduced perpendicularly into the flow tube.

Table 2
Rate coefficients of CO_3^- + HNO_3 reaction measured as a function of pressure

Pressure (hPa)	Rate coefficient[a]	No. of experiments
1.1	1.2 ± 0.2	9
1.9	1.2 ± 0.1	53
3.2	1.2 ± 0.2	9
4.8	1.2 ± 0.4	26
6.9	1.2 ± 0.3	3
11.8	0.9 ± 0.2	10
17.7	1.0 ± 0.1	5

[a] In units of 10^{-9} cm^3 s^{-1}. Confidence level of 95%.

All the results are presented in Table 2. No pressure effect on the rate coefficient was observed, within experimental uncertainties. Above 18 hPa, no rate coefficient could be measured, due to unstable and too low transmission of ions. We report a final room-temperature rate coefficient of $(1.2 \pm 0.3) \times 10^{-9}$ cm^3 s^{-1} for the CO_3^- + HNO_3 reaction, using the results at pressures below 7 hPa for which the flow dynamics is well defined and most of the experiments were performed. Quoted errors include both experimental scatter (10%) and systematic errors, combined by the method of propagation errors. The potential systematic errors were estimated to be 25%, including 10% for τ measurement, and 10% for each of the four parameters used in the determination of $[HNO_3]$ (see Sec. 2.4.). This rate coefficient was previously measured by Fehsenfeld et al. [13] at 0.5 hPa in He, and by Möhler and Arnold [14] at 2 hPa in N_2, relative to those of reactions of HNO_3 with Cl^- and O^-, respectively. Using the recent values of Huey [15] for these reference reactions, the rate coefficient values were corrected to (1.4 ± 0.4) and $(1.6 \pm 0.6) \times 10^{-9}$ cm^3 s^{-1}, respectively. So, the agreement is good with our value, which is the only one measured in an absolute way.

The rate coefficient was also determined at 212 ± 5 K. The flow tube was wrapped in dry ice, and temperature was measured by two Pt resistance probes with high temperature coefficient, installed in the first and third inlet ports, the second being used for

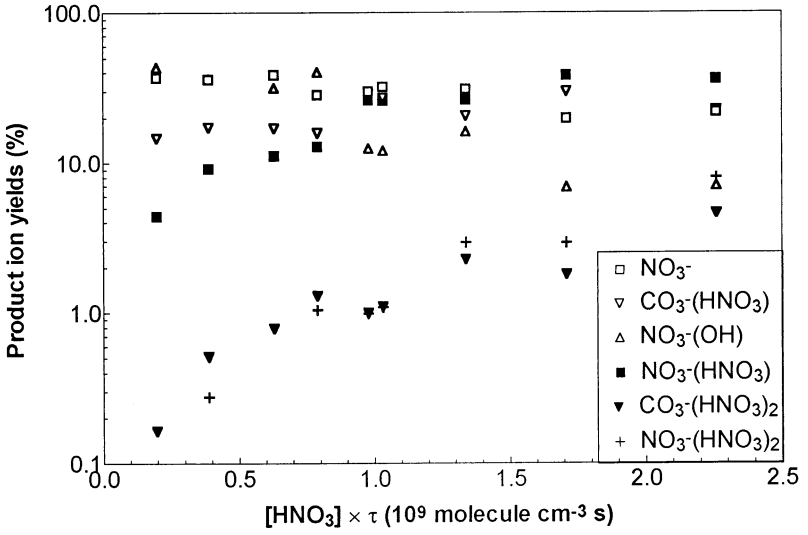

Fig. 4. Product ion distribution vs. $[HNO_3] \times \tau$ at 1.1 hPa and 298 K.

the introduction of HNO_3 (reaction distance of 47.5 cm). With a precooling zone of 100 cm for the carrier gas N_2 at 1.6 hPa, no difference of temperature (± 2 K) was observed between the two probes. However a temperature variation of ± 5 K in the flow tube arose from nonuniform sublimation of the dry ice in contact with the tube walls during the course of the experiments. Care was taken to avoid condensation of HNO_3 at the most critical point, namely inside the inlet port, by insulating this one from contact with dry ice. Otherwise, HNO_3 traces were detected by the presence of $CO_3^-(HNO_3)$ signal, when HNO_3 flow was stopped and only argon flow was passing through the absorption cell and the inlet. In spite of the low concentration (< 3 ppmv) of water contained in the carrier gas, $CO_3^-(H_2O)$ signal was observed. This may be explained by the faster reaction of CO_3^- with H_2O at lower temperatures, and may be by leaks occurring in the inlet zones containing the temperature probes, due to hardening or retraction of the O-rings used for the mounting of the temperature probes. However, the $CO_3^-(H_2O)$ concentration was low enough (< 0.1 $[CO_3^-]$) not to hinder rate coefficient measurements. From the plot of $\ln([CO_3^-]/[CO_3^-]_0)$ as a function of 13 different HNO_3 concentration values (1×10^8 to 2×10^9 cm^{-3}), a rate coefficient of (2.4 ± 0.7) × 10^{-9} cm^3 s^{-1} was deduced at 212 ± 5 K and 1.6 hPa. Under this experimental condition, no significant difference of the ratio V_i/V_g was observed, and the value reported in Table 1 was therefore used for deriving the reaction time. The quoted uncertainty includes both experimental scatter (15%) and potential systematic (25%) errors. At higher pressure (4.8 hPa for instance), comparable results were found, but we rejected them because a significant temperature gradient (10 K) arose. The order of magnitude of the rate coefficient (10^{-9} cm^3 s^{-1}) is typical of ion/molecule reactions, in which long-range attractive forces between ion and dipole dominate the activation barrier and make the encounter rate greater than the collision frequency for the neutrals. In this case, a negative temperature dependence of the rate coefficient may be observed [21].

3.2. Product ion distribution

Product ion distribution of the CO_3^- + HNO_3 reaction was investigated from 1 to 24.3 hPa. The study was performed at low resolution of the mass analyzer to limit mass discrimination, which usually underestimates ions of higher mass. Fig. 4 depicts the evolution of the product ion yields as a function of

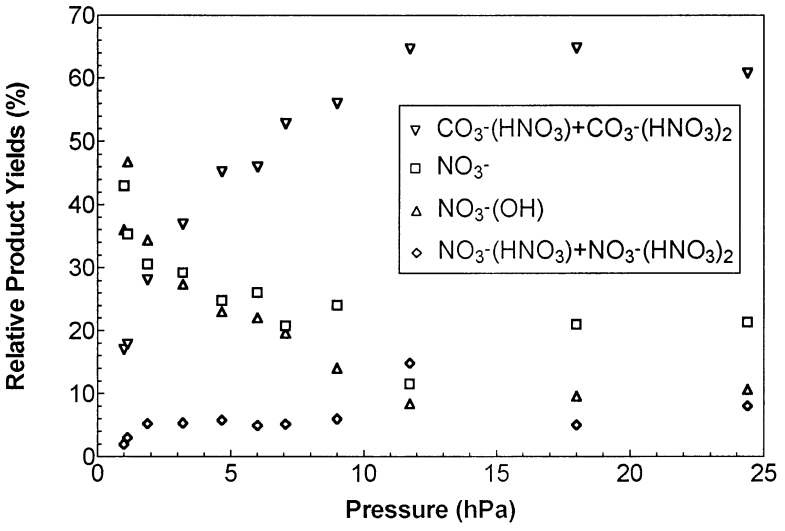

Fig. 5. Product ion distribution vs. pressure at 298 K.

$[HNO_3] \times \tau$, at a pressure of 1.1 hPa and room temperature, in order to distinguish primary from secondary product ions. The primary product ions observed were $CO_3^-(HNO_3)$, NO_3^-, and $NO_3^-(OH)$, since they are the more abundant at lower HNO_3 concentrations, and their yields decreased for higher $[HNO_3]$, which suggests further reactions of them with HNO_3. Identification of the product ions $CO_3^-(HNO_3)_2$, $NO_3^-(HNO_3)$, and $NO_3^-(HNO_3)_2$, whose relative yields increase with $[HNO_3]$, is consistent with the fact that these are formed as secondary products.

Fig. 5 shows the variation of the product ion yields as a function of pressure at room temperature. Uncertainty yields are 20%, deduced from experiments with various electrostatic conditions of ion transfer. During this experiment, the HNO_3 concentration was kept constant and below 10^{10} cm^{-3}, so that the product ions observed were mainly primary products. Product ion yields from 1 to 3 hPa are listed in Table 3, for comparison with Möhler and Arnold's data [14]. Similarly to their study, the three primary products were detected, and we observed the $CO_3^-(HNO_3)$ yield increasing from 17 to 37%. These yields are lower limits as they correspond to the product of highest mass, compared to NO_3^- and $NO_3^-(OH)$. In addition, Fig. 5 shows that the yield of $CO_3^-(HNO_3)$ + $CO_3^-(HNO_3)_2$ keeps increasing between 3 and 12 hPa, reaching at least 60% of the total product ions above 12 hPa. In parallel, the NO_3^- and $NO_3^-(OH)$ yields decreased down to $\leq$ 20% and $\leq$ 10%, respectively, with a constant yield of the secondary products $NO_3^-(HNO_3)$ and $NO_3^-(HNO_3)_2$ of about 10%. The temperature effect on the product distribution was also studied. The lowering of temperature has a clear repercussion: the yield of $CO_3^-(HNO_3)$ + $CO_3^-(HNO_3)_2$ increased from at least 55% at 1.1 hPa (205 K) to more than 85% between 6 hPa (212 K) and 20 hPa (234 K), as shown in Fig. 6. The NO_3^- signal remaining was assigned partially ($\approx$ 50%) to the reaction of HNO_3 with CO_4^-, also generated in the DIS. The temperature could not be maintained at 205 K when the carrier gas flow giving the pressure

Table 3
Relative yields (in %) of the product ions for the reaction of CO_3^- with HNO_3 as a function of pressure at 298 K

Product ions	1 hPa	2 hPa	3 hPa
$CO_3^-(HNO_3)$	17 (33)[a]	28 (43)	37 (47)
NO_3^-	43 (33)	31 (27)	29 (21)
$NO_3^-(OH)$	36 (34)	34 (30)	27 (32)
$NO_3^-(HNO_3)_{1 \text{ and } 2}$	2	5	5

[a] Values in parentheses are those from Möhler and Arnold [14].

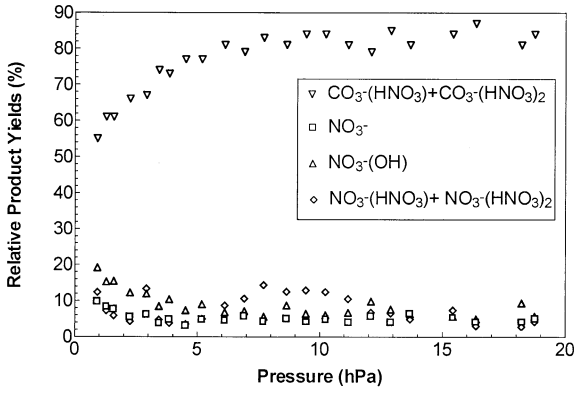

Fig. 6. Product ion distribution vs. pressure at 205–234 K.

increased, because the precooling was less and less effective. Formation in favor of $CO_3^-(HNO_3)$ as pressure increases or temperature decreases suggests that reaction channel leading to this product is globally termolecular.

The following reaction mechanism was proposed by Möhler and Arnold [14]:

$$CO_3^- + HNO_3 \underset{k_d}{\overset{k_a}{\rightleftharpoons}} CO_3^-(HNO_3)^* \xrightarrow[+N_2]{k_1} CO_3^-(HNO_3) \quad (1)$$

$$\xrightarrow{k_2} NO_3^- + CO_2 + OH \quad (2)$$

$$\xrightarrow{k_3} NO_3^-(OH) + CO_2 \quad (3)$$

These authors observed an increase of the $CO_3^-(HNO_3)$ yield relative to the NO_3^- yield with increasing pressures, and showed that collision-induced dissociation of $CO_3^-(HNO_3)$ resulted in the formation of CO_3^-, NO_3^-, and $NO_3^-(OH)$. This indicates that an indirect ion/molecule reaction takes place, with a common intermediate energized complex $CO_3^-(HNO_3)^*$. This one may be collisionally stabilized by N_2 [reaction (1) with the bimolecular rate coefficient k_1], decompose to products different from reactants [reactions (2) and (3) with the unimolecular rate coefficients k_2 and k_3, respectively], or redissociate to reactants [reaction (d) with the unimolecular rate coefficient k_d]. Using the steady-state approximation, the overall rate coefficient deduced is:

$$k = k_a \frac{k_1[N_2] + k_2 + k_3}{k_d + k_1[N_2] + k_2 + k_3}$$

The existence of the three primary product ions, $CO_3^-(HNO_3)$, NO_3^-, and $NO_3^-(OH)$, indicates that $k_1[N_2]$, k_2, and k_3 are competitive in the pressure range 1–24 hPa at room temperature. However, we observed no pressure effect on the rate coefficient, implying that the redissociation rate coefficient k_d is negligible, compared to the rate coefficient for the formation of products, $k_1[N_2] + k_2 + k_3$. The rate coefficient k measured in our work is thus simply equal to the rate coefficient k_a of the association reaction (a).

4. Conclusion

In the present work, we have demonstrated the ability of our new flowing-afterglow apparatus for kinetic studies of ion/molecule reactions over a range of pressures of 1.1–17.7 hPa. The rate coefficient of $CO_3^- + HNO_3$ reaction was measured in an absolute way for the first time, and its value, independent of pressure, is in good agreement with previous relative determinations restricted to pressure below 3 hPa. Above 20 hPa, no kinetic study could be performed because of too low ion transmission. To improve ion transmission, the pumping efficiency of the whole apparatus will be increased in the future. Product study was conducted between 1 and 24 hPa at room temperature, also corroborating a preceding work [14] in the sense that the product yields were of similar magnitude, as well as their evolution. Moreover, a lower limit of 60% was found above 12 hPa for the termolecular reaction channel, given by the product yield $CO_3^-(HNO_3) + CO_3^-(HNO_3)_2$.

Results obtained at low temperature allow data analysis of MACSIMS balloon flights. In this instrument, CO_3^- ions are used for the measurement of HNO_3 mixing ratio in the stratosphere [4,22]. The rate coefficient value of $(2.4 \pm 0.7) \times 10^{-9}$ cm^3 s^{-1} we

measured at 212 ± 5 K is directly applicable to data analysis obtained in the stratosphere where similar temperatures exist. The product study showed an increase of the $CO_3^-(HNO_3)$ yield to a value of more than 85% when pressure increases to 6 hPa. This suggests that reaction channel (1) proceeding by collisional stabilization is even more favored at the higher pressures (> 10 hPa) existing in the lower stratosphere (< 32 km altitude), where MACSIMS flights occur. In-situ data can thus be analyzed by neglecting channels (2) and (3). Indeed, no $NO_3^-(OH)$ was detected in the flight spectra. However, NO_3^- signal was present [23]. Since both these ions decreased in yields under low-temperature laboratory conditions, it seems reasonable to conclude that NO_3^- in-situ signal does not result from CO_3^- reaction with HNO_3. Reaction with other stratospheric trace gases, mainly NO_2 and $ClONO_2$, is a possibility, based on the mixing ratios and reaction rate coefficients of these species with CO_3^- ion [19,24].

Acknowledgements

We thank J. Lespagnol (LPCE) for helpful discussions and technical help, E. Arijs (BIRA) for helpful discussions and critical reviewing of the manuscript, C. Beaugrand for technical assistance. We thank the Commission of the European Communities (Environment and Climate Programme—contract no. ENV4 CT95 0042), and the Conseil Régional du Centre for financial support.

References

[1] F. Arnold, R. Fabian, G. Henschen, W. Joos, Planet. Space Sci. 28 (1980) 681.
[2] E. Arijs, D. Nevejans, J. Ingels, P. Frederick, Geophys. Res. Lett. 4 (1983) 329.
[3] F. Arnold, G. Knop, Int. J. Mass. Spectrom. Ion Processes 81 (1987) 33.
[4] C. Amelynck, E. Arijs, E. Neefs, D. Nevejans, W. Vanderpoorten, A. Barassin, C. Guimbaud, D. Labonnette, H.P. Fink, E. Kopp, H. Reinhard, in R.D. Bojkov, G. Visconti (Eds.), Proceedings 18th Quadriennal Ozone Symposium, L'Aquila, Italy, 12–21 September 1996, Parco Scientifico Technologico d'Abruzzo, pp. 453–456.
[5] C. Amelynck, E. Arijs, E. Neefs, D. Nevejans, N. Schoon, A. Barassin, V. Catoire, C. Guimbaud, D. Labonnette, H.P. Fink, U. Jenzer, E. Kopp, W. Luithardt, in N.R.P. Harris, I. Kilbane-Dawe, G.T. Amanatidis (Eds.), Proceedings 4th European Symposium on Stratospheric Ozone Research, Schliersee, Germany, 22–26 September 1997, Air Pollution Research Report 66, pp. 617–620.
[6] C. Rytz, E. Kopp, P. Eberhardt, Int. J. Mass. Spectrom. Ion Processes 137 (1994) 55.
[7] D. Fussen, C. Amelynck, E. Arijs, Int. J. Mass. Spectrom. Ion Processes 116 (1992) 13.
[8] C. Amelynck, D. Fussen, E. Arijs, Int. J. Mass. Spectrom. Ion Processes 133 (1994) 13.
[9] E.E. Ferguson, F.C. Fehsenfeld, A.L. Schmeltekopf, Adv. At. Mol. Phys. 5 (1969) 1.
[10] Y. Ikezoe, S. Matsuoka, M. Takebe, A.A. Viggiano, Gas Phase Ion-Molecule Rate Constants Through 1986, Maruzen, Tokyo, 1987.
[11] B.L. Upschulte, R.J. Shul, R. Passarella, R.G. Keessee, A.W. Castleman, Int. J. Mass. Spectrom. Ion Processes 75 (1987) 27.
[12] N.C. Adams, M.J. Church, D. Smith, J. Phys. D: Appl. Phys. 8 (1975) 1409.
[13] F.C. Fehsenfeld, C.J. Howard, A.L. Schmeltekopf, J. Chem. Phys. 63 (1975) 2835.
[14] O. Möhler, F. Arnold, J. Atm. Chem. 13 (1991) 33.
[15] L.G. Huey, Int. J. Mass. Spectrom. Ion Processes 153 (1996) 145.
[16] D.A. Dahl, J.E. Delmore, SIMION Version 4.0, Idaho National Engineering Laboratory, Idaho Falls, 1988.
[17] D. Smith, N.G. Adams, Adv. At. Mol. Phys. 24 (1988) 1.
[18] J.V. Seeley, J.T. Jayne, M.J. Molina, Int. J. Chem. Kinet. 25 (1993) 571.
[19] F.C. Fehsenfeld, E.E. Ferguson, J. Chem. Phys. 61 (1974) 3181.
[20] W.B. DeMore, S.P. Sander, D.M. Golden, R.F. Hampson, M.J. Kurylo, C.J. Howard, A.R. Ravishankara, C.E. Kolb, M.J. Molina, NASA JPL publication 94-26, Jet Propulsion Laboratory, Pasadena, 1994.
[21] I. W. Smith, Int. J. Mass Spectrom Ion Processes 149 (1995) 231.
[22] C. Guimbaud, Ph.D. Thesis, Université d'Orléans, Orléans, 1997.
[23] E. Arijs, A. Barassin, E. Kopp, C. Amelynck, V. Catoire, H.P. Fink, C. Guimbaud, U. Jenzer, D. Labonnette, W. Luithardt, E. Neefs, D. Nevejans, N. Schoon, A.M. Van Bavel, Int. J. Mass Spectrom. Ion Processes, in press.
[24] A.A. Viggiano, R.A. Morris, J. Geophys. Res. 99 (1994) 8221.